Science & Technology Development Journal – Engineering and Technology, 5(2):1426-1436

Open Access Full Text Article

Research Article

Simulating the piezoelectric substrate influence on the characteristics of surface acoustic wave-magnetostriction sensor based on the FeNi magnetic sensitive material

Do Duy Phu[1,2,*], Hoang Si Hong[1,*], Le Van Vinh[3]

Use your smartphone to scan this QR code and download this article

ABSTRACT

This paper simulates the influence of two piezoelectric substrate types on the sensitivity and measuring range of surface acoustic wave-magnetostriction (SAW-MO) sensor by the finite elements method (FEM) based on using the FeNi magnetic sensitive layer with E-H chacrateristics (Young's Modulus – Magnetic field intensity). The sensor structure selected for the study is the delay-line: the distance between the two sets of electrodes is 5mm, the number of finger pairs of each electrode set is 25, and the distance-width between the fingers is 10mm regularly, the electrode material is aluminum. The piezoelectric substrates chosen for simulation are $LiNbO_3$ and AlN in which the $LiNBO_3$ piezoelectric substrate is the block form with the surface velocity of 3318.1m/s and the AlN piezoelectric substrate is the thin film with the surface wave velocity of 5598.9m/s. So the generality is ensured when evaluating their influence on the response of SAW-MO sensor. For magnetic sensitive materials, the group selected the FeNi which E-H characteristics was experimentally built. During simulation by finite elements method, the sensor structure is tested with many datasets whose number of divided elements is different. However, the simulation results have converged with the number of divided elements is 113556. The simulation result shows that the sensivity of the FeNi/IDT/AlN structure magnetic sensor is larger than the FeNi/IDT/$LiNbO_3$ structure magnetic sensor with sensitivities of 8.698kHz/Oe and 2.345kHz/Oe, respectively. The result also indicates that the response range of the FeNi/IDT/AlN magnetic sensor is [0 ÷ 109]Oe, which is smaller than the FeNi/IDT/$LiNbO_3$ magnetic sensor is [0 ÷ 190]Oe.

Key words: SAW, FEM, Surface Acoustic Wave, Finite elements method, Surface Acoustic Wave – Magnetostrictive, The characteristics of SAW-MO sensor

[1]*School of Electrical and Electronic Engineering, Hanoi University of Science and Technology, Hanoi, Vietnam*

[2]*Hanoi University of Industrial, Hanoi, Vietnam*

[3]*Phenikaa University, Hanoi, Vietnam*

Correspondence

Do Duy Phu, School of Electrical and Electronic Engineering, Hanoi University of Science and Technology, Hanoi, Vietnam

Hanoi University of Industrial, Hanoi, Vietnam

Email: doduyphu@haui.edu.vn

Correspondence

Hoang Si Hong, School of Electrical and Electronic Engineering, Hanoi University of Science and Technology, Hanoi, Vietnam

Email: hong.hoangsy@hust.edu.vn

History

- Received: 22-11-2021
- Accepted: 26-4-2022
- Published: 30-6-2022

DOI : 10.32508/stdjet.v5i2.945

Check for updates

INTRODUCTION

The sensor uses the surface acoustic wave (SAW) effect with the advantages such as high sensitivity, easy fabrication, so that it has been widely applied to measure physical quantities such as temperature, concentration, current, deformation, magnetic field intensity, ...[1–6]. Recently, the magnetic sensors with SAW structure have been studied by many groups because of their important role in many applications[3,4,6–8]. In fact, the magnetic sensors operate basing on different physical effects or the combination of many physical effects. Magnetoelectric effect (ME) is a combination of magnetostriction effect and piezoelectric effect with sandwich structure, the studies often use three material layers (such as: Terfenol-D/PZT/Terfenol-D, Fe/P/Fe,...) in which the middle layer is piezoelectric material, the upper and lower layers are magnetostrictive materials, and this structure, the sensor gives the output of voltage response[9,10]. Another popular combination is to use the surface acoustic wave on the piezoelectric material combined with the magnetostrictive material by delay-line structure, which creates a magnetic sensor with large sensitivity and high working frequency[1,4,10]. Optimizing the structure and improving the response of the sensor have been performed by many research groups. The study[11] selects to change the material type in the intermediary layer of the magnetic sensitive layer and the piezoelectric substrate with two structures Ni/Al_2O_3/IDT/$LiNbO_3$ and Ni/ZnO/IDT/$LiNbO_3$. The result reflects that the structure using the $Al2O_3$ intermediary layer has larger sensitivity than the structure using the ZnO intermediary layer does. Another study chose to use LOVE wave, with FeCoSiB/SiO_2/IDT/ST-cut Quartz structure to detect the biomagnetic field[7]. Recently, the research[6] changes the aspect factor ($p = l/w$ is the ratio of length to width) of the sensitive layer to optimize the sensor's response on the FeNi/ZnO/IDT/YZ-$LiNbO_3$ structure. By the way of uniting the CHRISTOFFEL equation to solve the elec-

Cite this article : Phu D D, Hong H S, Vinh L V. **Simulating the piezoelectric substrate influence on the characteristics of surface acoustic wave-magnetostriction sensor based on the FeNi magnetic sensitive material**. *Sci. Tech. Dev. J. – Engineering and Technology;* 5(2):1426-1436.

tromechanical equations which were made for the layers of the sensor, the solution process involves a lot of equations and combines many complex boundary conditions, and the research also indicates the good results.

Thus, with the SAW-magnetostriction sensor structure, the study of the direct influence of the piezoelectric substrate on the sensor's working response has not been mentioned in many researchs. Accordingly, in this study, we simulate the influence of piezoelectric substrates on the SAW-magnetostrictoin sensor characteristics with AlN piezoelectric substrate and $LiNbO_3$ piezoelectric substrate. The AlN piezoelectric substrate was chosen because of its high surface wave velocity (over 5000 m/s) that has the potential for large sensitivity [5,12]. Besides, the FeNi material has been proven to have good magnetostriction and high sensitivity [6,13,14], so it should be selected as a magnetic sensitive material in this study. Recently, the simulation of the finite elements method (FEM) through commercially available softwares have been applied by many groups for many different applications such as: [11] sensor simulation, and our research team has successed with studies about SAW resonator and SAW filter [15,16]. The advantage of this method is that it allows simulating directly the magnetic SAW sensor structure with parameters such as: electrode shape (IDT: inter-digital transducer), piezoelectric substrate type, magnetic sensitive layer. Preparing a set of material parameters is not complicated, the simulation results are visualized in the image and the wave, the response can be analyzed into frequency, amplitude or phase which are fairly accurate in comparison with the experimental results [17].

Basing on the above information, in this paper, we use the FEM to simulate and evaluate the combination of FeNi sensitive layer with the piezoelectric substrates are AlN thin-film and LiNbO3 bulk. The E-H [6,13] characteristics were used to calculate the simulation input data set for FeNi magnetic sensitive material when the magnetic field intensity changes in the working range.

RESEARCH METHODS

Principle and structure of the sensor

A type of SAW device has the structure shown in Figure 1. The structure includes: The device consists of a piezoelectric (PE) substrate; two electrode sets are placed on the substrate, the input IDT (IDT-in) is on the left, the output IDT (IDT-out) is on the right; a delay-line is between the two IDTs, the delay-line acts as a sensitive area and will change the velocity, amplitude, and phase of the surface acoustic wave when moving through this region. Applying a voltage into the input IDT creates a surface acoustic wave on the piezoelectric substrate with the reverse piezoelectric effect. The surface acoustic wave propagates through the delay-line to the output IDT, in which a forward piezoelectric effect occurs. That means the voltage is produced on the output IDT. This signal will be changed in frequency (proportional to the velocity of surface acoutic wave), wave amplitude when the delay-line part interacts with the quantity that needs to be measured.

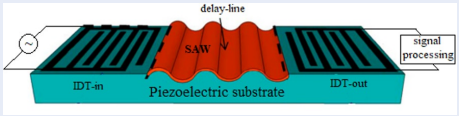

Figure 1: The structure of SAW device [6].

From the above principle, the magnetic sensor structure (Figure 2) which is proposed for research has the delay-line form with wavelength $\lambda = 40\mu$m, magnetic sensitive layer using FeNi alloy with fixed thickness of h3 = 1μm and the structural parameters are shown in Table 1 specifically and the magnetic field intensity (H) is the measured signal.

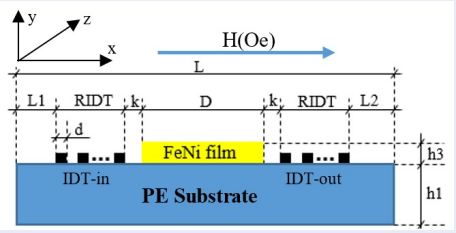

Figure 2: The structure of SAW-MO sensor.

FEM simulation model

The operating principle of the SAW-MO sensor is based on the surface acoustic wave effect being combined with the magnetostriction effect when coupling a piezoelectric material layer using AlN and $LiNbO_3$ with a magnetic sensitive material layer (FeNi). The piezoelectric effect occurs on the piezoelectric material according to the Hook's law that is represented through the relationship of Stress (**T**), strain (**S**), Electric field (**E**) and Electric displacement field (**D**), as follows [18,19].

$$\begin{aligned} \mathbf{T} &= c_E\mathbf{S} + e^T\mathbf{D} \\ \mathbf{D} &= e\mathbf{S} - \varepsilon\mathbf{E} \end{aligned} \quad (1)$$

Table 1: Structural parameters of the magnetic sensor

NO	Parameters	Value (μm)
1	Number of IDT finger pair: n	25 pairs
2	Width of each finger: d	10
3	Left edge distance: L1	2000
4	Right edge distance: L2	2000
5	Length of IDT: RIDT	990
6	Length of magnetic sensitive layer: D	4960
7	Thickness of piezoelectric layer: h1	400
8	Thickness of magnetic sensitive layer: h3	1
9	Gap between IDT and sensitive layer: k	20
10	Sensor length: L	10980

Where: c_E, e and ε are the elastic stiffness matrix, piezoelectric matrix and dielectric matrix in consequence; These constants are shown in Table 2.

According to [18] there is the motion equation of particle in the solid:

$$\nabla \cdot \mathbf{T} = \rho \frac{\partial^2 \mathrm{u}}{\partial \mathrm{t}^2} \text{ or } \nabla \cdot \mathbf{T} = \rho \frac{\partial \mathrm{v}}{\partial \mathrm{t}} \quad (2)$$

and

$$\mathbf{E} = -\nabla\phi \quad (3)$$

Where: u is displacement of the particle in the solid, v is the velocity of the phase or the velocity of wave propagation, and ϕ is the potential.

and the operators [18]:

$$\nabla = \begin{bmatrix} \frac{\partial}{\partial x} & \frac{\partial}{\partial y} & \frac{\partial}{\partial z} \end{bmatrix}$$

$$\nabla\cdot = \begin{bmatrix} \frac{\partial}{\partial x} & 0 & 0 & 0 & \frac{\partial}{\partial z} & \frac{\partial}{\partial y} \\ 0 & \frac{\partial}{\partial y} & 0 & \frac{\partial}{\partial z} & 0 & \frac{\partial}{\partial x} \\ 0 & 0 & \frac{\partial}{\partial z} & \frac{\partial}{\partial y} & \frac{\partial}{\partial x} & 0 \end{bmatrix}$$

Combining (2), (3) with (1) under the condition $\nabla\cdot \mathbf{D} = 0$ we can represent the relationship (1) into the constitutive equations (4) in the index form, and according to [6,18], there is:

$$\begin{cases} \rho \frac{\partial^2 u_i}{\partial^2 t^2} - \nabla_{ik} c_{KL} \nabla_{Lj} u_j - \nabla_{ik} e_{Kj} \nabla_j \phi = 0 \\ \nabla_i e_{iL} \left(\nabla_{Lj} u_j\right) - \nabla_i \varepsilon_{ij} \nabla_j \phi = 0 \end{cases} \quad (4)$$

Where: $i, j, k, l = x, y, z$; $K = ij$, $L = kl$ ($K, L = 1, 2, 3, 4, 5, 6$). The constitutive equations (4) reflect the relationship between the forward piezoelectric effect and the reverse piezoelectric effect; indicate the influence of density (ρ), elastic stiffness coefficient (c_{KL}), … of the propagation medium on the velocity, amplitude, and phase of the acoustic wave.

The above model [the equations (4) and data in Table 2] is solved by FEM through simulation steps performed as follows: Declaring the structure and entering the physical parameters [elastic coefficients (c_{KL}), piezoelectric coefficients (e_{ij}), Young's module (E),...] for material layers, building sensor structure (Figure 2), meshing, changing material layers, applying the voltage on IDT-in and setting the boundary conditions. The process of performing FEM simulation is shown in Figure 3 and is performed on the simulation software of the finite elements method that is similar to previous publications by our group [15,16].

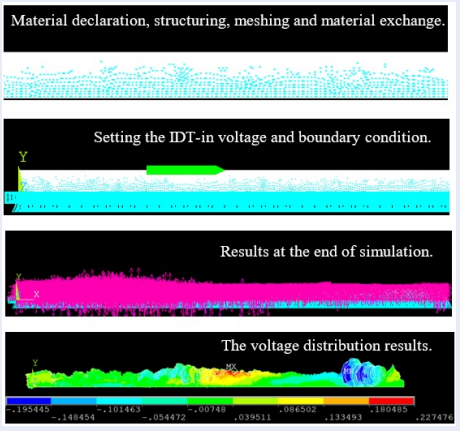

Figure 3: The images performed by the FEM simulation process.

With meshing to make the simulation process faster but still ensuring the accuracy, the IDTs and FeNi sensitive layer are located on the upper surface of the sensor where the meshing density is thick and then sparse

Table 2: Physical parameters of piezoelectric materials (AlN, $LiNbO_3$), Aluminum (Al) and FeNi [6,12,19–22].

Material parameters		Value			
		AlN	$LiNbO_3$	Al	FeNi
Elastic stiffness coefficients (10^{11}N.m^{-2})	C_{11}	4.10	1.986		
	C_{12}	1.49	0.547		
	C_{13}	0.99	0.752		
	C_{14}	3.89	0.085		
	C_{33}	1.25	2.424		
	C_{44}		0.595		
Piezoelectric coefficients (C.m^{-2})	e_{11}	0.58	3.76		
	e_{13}	1.55	-2.43		
	e_{15}	0.48	0.23		
	e_{16}		1.33		
	e_{24}				
	e_{31}				
	e_{33}				
Dielectric constants	ε_{11}	9.0	38.9		
	ε_{22}	9.0	38.9		
	ε_{33}	9.0	38.9		
Density (kg.m^{-3})	ρ	3300	4700	2697	8380
Young's modulus (GPa)	E			70.3	E-H
Poison ratio	v			0.345	0.3

gradually to the bottom of the sensor. The meshing step applied is $\lambda/40 = 1\mu$m, after dividing the element number of the model is 113556, the simulation results are guaranteed to be converged. The specific boundary conditions are as follows: The top surface of sensor has the free mechanical condition and the zero voltage. Its bottom has the fixed mechanical condition, and the voltage condition is grounded. The junction between two materials has free mechanical condition and continuous voltage. All side edges of the sensor have free condition.

The process of FEM calculation performs as follows: Applying a square pulse voltage into the IDT-in with 100V amplitude, 20ns pulse width. The calculation time is enough for the surface acoustic wave to propagate from IDT-in to IDT-out that is 1500ns, the cycle of signal sampling is 0.3ns which satisfies Shannon's theorem. The output voltage is read at the IDT-out in the time domain, then converted to the frequency domain by the FFT (Fast Fourier Transform) spectral density transform algorithm to determine the SAW velocity, the resonant frequency (f) and the frequency shift ($\triangle$f) when the input signal (H) of the sensor changes. This process is performed iteratively at each point on the sensor characteristic (H-f: is the relationship between the input signal H and the output signal f of the sensor).

Analysis of the relationship between magnetic field intensity and SAW velocity

According to the theory of wave propagation in the elastic materials, there are many types of different wave, this research studies the Rayleigh wave, and according to [23,24], there is a relationship of wave propagation velocity between Rayleigh wave (V_R) and shear wave (V_S), that is (5).

$$\frac{V_R}{V_S} = \frac{0.436 + c_{12}/c_{11}}{0.5 + c_{12}/c_{11}} \approx \left[\frac{2}{A}\left(1 - \frac{c_{66}}{Ac_{11}}\right)\right]^{1/2} \quad (5)$$

where: Anisotropic factor $A = 2c_{44}/(c_{11} - c_{12})$ and $V_S = \sqrt{c_{66}/\rho}$ or $V_S = \sqrt{c_{44}/\rho}$ (if $c_{66} = c_{44}$) [10,11] with $c_{66} = (c_{11} - c_{12})/2$ [18], applied in this study, is the density of the wave propagation medium layer. Thus, we recognize that the Rayleigh wave velocity or SAW velocity depends on the mechanical properties of the wave propagation medium, such as density (ρ) and elastic stiffness coefficient (c_{44} hoặc c_{66}). According to the sensor structure proposed (Figure 1), the SAW velocity is affected by the density and elastic stiffness coefficient of the wave propagation medium, that includes the piezoelectric (PE) material layer and the magnetic sensitive layer (FeNi).

The FeNi magnetic sensitive material layer has the elastic stiffness coefficients determined as follows[6]:

$$\begin{cases} c_{11}^F = \dfrac{E(1-v_F)}{(1+v_F)(1-2v_F)} \\ c_{12}^F = \dfrac{Ev_F}{(1+v_F)(1-2v_F)} \\ c_{11}^F = \dfrac{E(1-2v_F)}{2(1+v_F)(1-2v_F)} \end{cases} \quad (6)$$

where: E is Young' modulus and the Poison coefficient of FeNi $v_F = 0.3$.

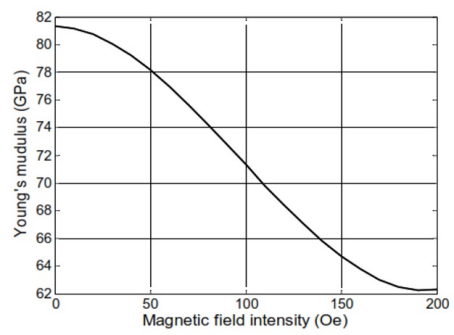

Figure 4: The E-H characteristic of the FeNi magnetic sensitive layer[6,13].

Besides, the E-H characteristic of the FeNi magnetic sensitive layer is measured by laser resonance method, this relationship shows that when the external magnetic field intensity (H: measured magnetic field intensity) changes, the Young's modulus (E) changes, too. This relationship is detailly shown in Figure 4[6,13]. Thus, using the above equations and combining with the E-H characteristics, we can determine the shift of the SAW velocity ($\triangle V_R$) when the external magnetic field intensity changes.

Finally, when combining the relation $\triangle V_R/V_R = \triangle f/f_0$[25] ($f_0$ is the central frequency of the sensor when H = 0Oe), it is founded that the working characteristics of the magnetic sensor with the input signal is the magnetic field intensity (H) and the signal output is the frequency (f). On the other hand, when determining the frequency (f) of the voltage at the sensor's IDT-out and using the FFT spectral density transform algorithm, the value of the magnetic field intensity (H) is measured.

RESULTS AND DISCUSSION

Figure 5 and Figure 6 show sequently the central frequency (f_c) responses of magnetic sensors of two structures which use the AlN and $LiNbO_3$ substrate, without the sensitive layer (point A), with the FeNi sensitive layer (point B) but no external magnetic field intensity H = 0(Oe), and with the maximum external magnetic field intensity (point C) respectively. We see that the resonant frequencies at points A and B are different (with frequency shift). This can be explained by two basic reasons. Firstly, when coating the magnetic sensitive layer (FeNi), the mass of FeNi makes the resonant frequency decrease[6,18]. Secondly, an increase in the acoustic wave velocity (asymptotically to the shear wave velocity) leads to an increase in the resonant frequency[18,23,24]. Thus, depending on the properties of the wave propagation medium, when the magnetic sensitive layer is coated without external magnetic field intensity, the resonant frequency will increase or decrease a bit compared to the resonant frequency when there is no magnetic sensitive layer. The frequency shift process (at the resonance peaks on the spectral density) of the sensors when the magnetic field intensity measured changes in the working range of the sensors can be seen more clearly in the Figure 7 and Figure 8.

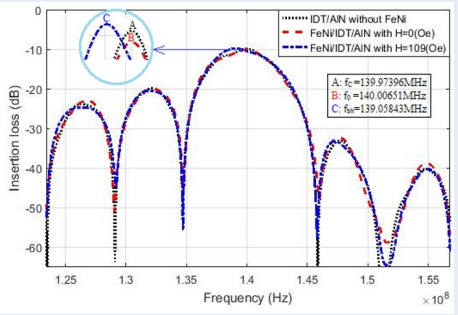

Figure 5: The frequency response of magnetic sensor with FeNi/IDT/AlN structure.

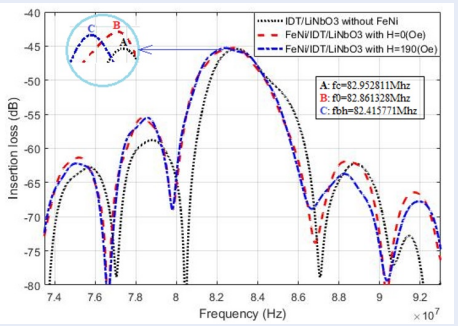

Figure 6: The frequency response of magnetic sensor with FeNi/IDT/$LiNbO_3$ structure.

The results state that the central resonant frequencies for IDT/AlN and IDT/$LiNbO_3$ structures are

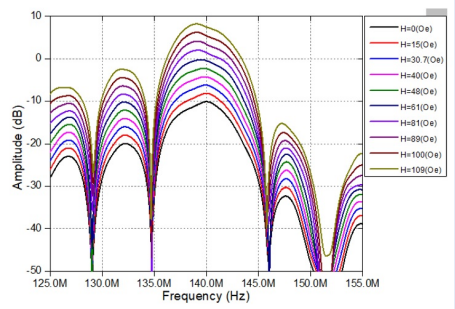

Figure 7: The frequency response at working points of magnetic sensor: FeNi/IDT/AlN.

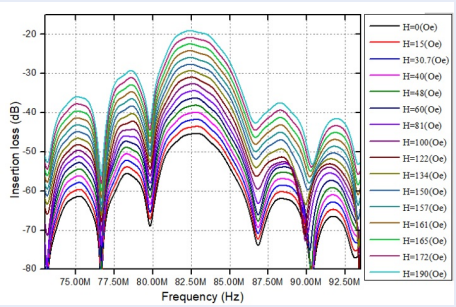

Figure 8: The frequency response at working points of magnetic sensor: FeNi/IDT/$LiNbO_3$.

139.97MHz and 82.95MHz, respectively. Thus, the SAW velocity V = λ*fc of the two structures IDT/AlN and IDT/$LiNbO_3$ are 5598.9m/s and 3318.1m/s, respectively, these results are suitable for[12,20]. On the other hand, according to the mechanical parameters in Table 2 and the theoretical basis of surface acoustic wave in Section "**Analysis of the relationship between magnetic field intensity and SAW velocity**", we determine the SAW velocity on two structures IDT/AlN and IDT/LiNbO3 as follows:

If V_{Ra} and V_{Rl} are the SAW velocity of two IDT/AlN and IDT/$LiNbO_3$ structures, V_{Sa} and V_{Sl} are the shear wave velocity of two IDT/AlN and IDT/$LiNbO_3$ structures. With $V_S = \sqrt{c_{66}/\rho}$, we have V_{Sa} = 6288.52m/s and V_{Sl} = 3911.25m/s. Thus, according to (5) we have V_{Ra} = 5822.39m/s and V_{Rl} = 3588.43m/s. So, when comparing the SAW velocity between the simulation results and the theoretical calculation results with an error (γ) and following the calculation below, we get the acceptable results:

γ_{Ra} = ((5822.39-5598.9)/ 5822.39) *100% = 3.84%

γ_{Rl} = ((3588.43-3318.1)/ 3588.43) *100% = 7.53%

Besides, the central frequency values of point B and point C in Figure 5 and Figure 6 shows that both FeNi/IDT/AlN and FeNi/IDT/LiNbO3 structures have the quite large shift of the central resonance frequency when applying the external magnetic field intensity to the sensors. To obtain the sensor responses in working range, more specifically: We change the magnetic field intensity H from 0(Oe) to 200(Oe) and divide into 16 points as shown in Table 3, through the E-H characteristic we can determine the Young's modulus values E to apply to the simulation. We simulate a point on the sensor response each time, the getting result is the voltage on the IDT-out and this is analyzed into the spectral density for determining the resonant frequency at the simulation point. As the results of spectral density analysis are shown in Figure 5 and Figure 6, point B gives the resonant frequency (f_0: center frequency) at the beginning point of the scale (H = 0Oe), point C indicates the resonant frequency (f_{bh}: saturation frequency) at the end point of the measuring scale. Specific results, the FeNi/IDT/AlN sensor structure gets f_0 = 140.00651Mhz and f_{bh} = 139.05843Mhz, and the FeNi/IDT/$LiNbO_3$ sensor structure gets f_0 = 82.861328Mhz and f_{bh} = 82.415771Mhz. The above process is performed at 16 points repeatedly for two FeNi/IDT/AlN and FeNi/IDT/$LiNbO_3$ structures. The final results are shown in Table 3. The working responses are plotted in Figure 9 and Figure 10 (showing the response of two sensor types with FeNi/IDT/AlN and FeNi/IDT/$LiNbO_3$ structures).

The working responses also give the results which are similar to the publications[6,8,11]. On the other hand, the response indicates that the FeNi/IDT/$LiNbO_3$ structure has the slower and larger magnetic saturation than the FeNi/IDT/AlN structure does. The sensor response detail with FeNi/IDT/AlN structure, when the measured signal of the sensor is the magnetic field intensity increases from beginning to the end of the scale (H = [0 ÷ 109]Oe) then the output frequency will decrease from the central frequency f_0 = 140.00651Mhz to the saturation frequency f_{bh} = 139.05843Mhz, or the frequency shift △f = [0 ÷ -948.08]kHz, and be clearly shown in Figure 9, Figure 11 and Table 3.

Similar to the sensor with FeNi/IDT/$LiNbO_3$ structure which gives the respone when the input signal is H = [0 ÷ 190]Oe and the output frequency is f = [82.861328 ÷ 82.415771]MHz, or the frequency shift is △f = [0 ÷ -445.557]kHz, that is clearly shown in Figure 10, Figure 11 and Table 3.

Thus, it is recognized that the FeNi/IDT/AlN sensor structure has the smaller measuring range than the FeNi/IDT/$LiNbO_3$ sensor structure (Figure 11).

Table 3: The frequency/magnetic field intensity response of the sensor with FeNi/IDT/AlN and FeNi/IDT/$LiNbO_3$ Structures.

NO	FeNi/IDT/AlN			FeNi/IDT/$LiNbO_3$		
	H(Oe)	f(hz)	△f(hz)	H(Oe)	f(hz)	△f(hz)
1	0.0	140006510	0	0.0	82861328	0
2	15.0	139990230	-16280	15.0	82855225	-6103
3	30.7	139908850	-97660	30.7	82827759	-33569
4	40.0	139827470	-179040	40.0	82806396	-54932
5	48.0	139729820	-276690	48.0	82785034	-76294
6	61.0	139497880	-508630	60.0	82736206	-125122
7	81.0	139192710	-813800	81.0	82659912	-201416
8	89.0	139119470	-887040	100.0	82586670	-274658
9	100.0	139074710	-931800	122.0	82504272	-357056
10	109.0	139058430	-948080	134.0	82467651	-393677
11	-	-	-	150.0	82440186	-421142
12	-	-	-	157.0	82431030	-430298
13	-	-	-	161.0	82424927	-436401
14	-	-	-	165.0	82421875	-439453
15	-	-	-	172.0	82418823	-442505
16	-	-	-	190.0	82415771	-445557

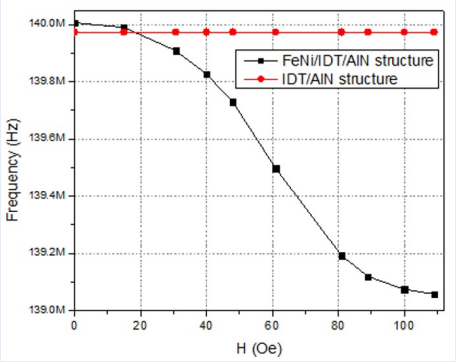

Figure 9: The working respone of magnetic sensor when using AlN substrate.

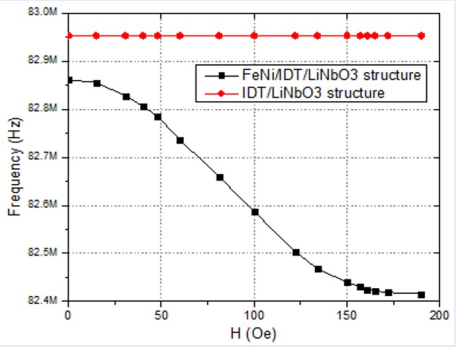

Figure 10: The working respone of magnetic sensor when using $LiNbO_3$ substrate.

Calculating the sensor sensitivities, the FeNi/IDT/AlN structure has the working range with [0 ÷ 109]Oe, the sensitivity is 8.698 (kHz/Oe); the FeNi/IDT/$LiNbO_3$ structure has the working range with [0 ÷ 190]Oe, the sensitivity is 2,345 (kHz/Oe). The influence of SAW velocity on sensor sensitivity is explained as follows. We know the shear wave velocity $V_S = \sqrt{c_{66}/\rho}$, which means that it is proportional to the elastic stiffness coefficient (stiffness) of the propagation medium, according to Table 2, the c_{66} of AlN is larger than the c_{66} of $LiNbO_3$, therefore the wave velocity of AlN material is faster than the wave velocity of $LiNbO_3$, this is suitable to [12,22]. Here, the propagation medium of two sensors are the FeNi/AlN and FeNi/$LiNbO_3$ coupling materials, so that the stiffness of the propagation medium is the equivalent stiffness of those coupling

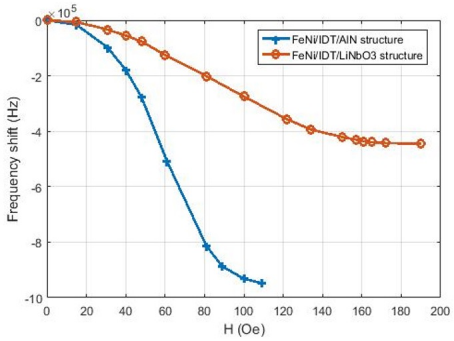

Figure 11: The frequency shift response of magnetic sensors with FeNi/IDT/AlN and FeNi/IDT/$LiNbO_3$ structures.

materials. When applying the external magnetic field intensity to the FeNi layer increases, the stiffness of this layer decreases [According to formula (6) and E-H characteristic Figure 4], This cause for the equivalent stiffness of the FeNi/AlN coupling decreases faster than the FeNi/$LiNbO_3$ coupling. Lead to, the SAW velocity on the FeNi/IDT/AlN sensor decreases faster than the SAW velocity on the FeNi/IDT/LiNbO3 sensor, when the magnetic field intensity changes the same (△H), shown in Table 4. On the other hand, we have $\triangle V_R/V_R = \triangle f/f_0$ [25]. Thus, we can see that the above simulation results are suitable to the theoretical basis, that the sensor structure uses AlN piezoelectric material has the higher SAW velocity than the $LiNbO_3$ piezoelectric material will give the sensor response has the higher sensitivity.

CONCLUSIONS

This work has simulated the magnetic sensor by FEM for two FeNi/IDT/AlN and FeNi/IDT/$LiNbO_3$ sensor structures. The FeNi/IDT/$LiNbO_3$ sensor structure has the measuring range of H = [0 ÷ 190] Oe and the sensitivity of 2,345 (kHz/Oe); the FeNi/IDT/AlN sensor structure has the measuring range of H = [0 ÷ 109] Oe and the sensitivity of 8.698 (kHz/Oe). The sensor's sensitivity increases 3.71 times by replacing the piezoelectric material from LiNbO3 to AlN in the magnetic sensor structure. On the other hand, the measuring range of the magnetic sensor decreases with replacing the piezoelectric material from $LiNbO_3$ to AlN. These results indicated that the SAW velocity affects on the sensitivity and measuring range of the SAW-MO sensor initially. We note that the research has not yet optimized the structure aspect of the sensor as well as the thickness of the sensitive layer, and the addition of the insulating layer between two piezoelectric and magnetic sensitive layers. The optimation will be considered in the future work.

ACKNOWLEDGMENTS

This research is funded by Vietnam National Foundationfor Science and Technology Development (NAFOSTED) under grant number 103.02-2018.33.

ABBREVIATIONS

SAW : Surface acoustic wave
SAW-MO : Surface acoustic wave-magnetostriction
FEM : Fininte elements method
ME : Magnetoelectric
PE : Piezoelectric
IDT : Inter-digital transducer
FFT : Fast fourier transform

COMPETING INTERESTS

The authors declare that there is no conflict of interest regarding the publication of this article.

AUTHORS' CONTRIBUTIONS

Do Duy Phu has simulated the working process of SAW-MO sensor and written the manuscript.
Hoang Si Hong has built the ideas and revised the manuscript.
Le Van Vinh has revised the manuscript and built the next development direction.

REFERENCES

1. Wang W, Jia Y. Development of a novel SAW Current Sensor Based on the Magnetostrictive Effect, IEEE International Ultrasonics Symposium Proceedings, 2015;Available from: https://doi.org/10.1109/ULTSYM.2015.0354.
2. Stoney R. Dermot Geraghty and Garret E. O'Donnell, Characterization of Differentially Measured Strain Using Passive Wireless Surface Acoustic Wave (SAW) Strain Sensors, IEEE SENSOR JOUNAL, VOL.14, NO.3, MARCH 2014;Available from: https://doi.org/10.1109/JSEN.2013.2285722.
3. Reindl LM, Shrena IM. Wireless Measurement of Temperature Using Surface Acoustic Wave Sensors, IEEE TRANSACTIONS ON ULTRSONICS, VOL.51, NO.11, NOVEMBER 2004;PMID: 15600090. Available from: https://doi.org/10.1109/TUFFC.2004.1367486.
4. Elhosni M, Elmazria O. FEM modeling of Multilayer Piezomagnetic Structure Based Surface Acoustic Wave Devices for Magnetic Sensor, ELSEVIER, EUROSENSOR 2014;Available from: https://doi.org/10.1016/j.proeng.2014.11.276.
5. Ha NH, Hong HS. Hydrogen Gas Sensing Using Palladium-Graphene Nanocomposite Material Based on Surface Acoustic Wave, Jounal of Nanomaterial, 2017;Available from: https://doi.org/10.1155/2017/9057250.
6. Tong J, Jia Y. Development of a Magnetostrictive FeNi Coated Surface Acoustic Wave Curent Sensor, Appl. Sci. 2017;Available from: https://doi.org/10.3390/app7080755.
7. Schell V, Müller C. Magnetic anisotropy controlled FeCoSiB thin films for surface acoustic wave magnetic field sensors, Applied Physics Letters, 2020;Available from: https://doi.org/10.1063/1.5140562.

Table 4: The SAW velocity/magnetic field intensity response of the sensor with FeNi/IDT/AlN and FeNi/IDT/$LiNbO_3$ Structures (with $V_R = \lambda * f$, λ=4*d and Table 3), $\triangle V_R$ is the shift velocity.

NO	FeNi/IDT/AlN			FeNi/IDT/LiNbO3		
	H(Oe)	V_R(m/s)	$\triangle V_R$(m/s)	H(Oe)	V_R(m/s)	$\triangle V_R$(m/s)
1	0.0	5600.26	0.00	0.0	3314.45	0.00
2	15.0	5599.61	-0.65	15.0	3314.21	-0.24
3	30.7	5596.35	-3.91	30.7	3313.11	-1.34
4	40.0	5593.10	-7.16	40.0	3312.26	-2.20
5	48.0	5589.19	-11.07	48.0	3311.40	-3.05
6	61.0	5579.92	-20.35	60.0	3309.45	-5.00
7	81.0	5567.71	-32.55	81.0	3306.40	-8.06
8	89.0	5564.78	-35.48	100.0	3303.47	-10.99
9	100.0	5562.99	-37.27	122.0	3300.17	-14.28
10	109.0	5562.34	-37.92	134.0	3298.71	-15.75
11	-	-	-	150.0	3297.61	-16.85
12	-	-	-	157.0	3297.24	-17.21
13	-	-	-	161.0	3297.00	-17.46
14	-	-	-	165.0	3296.88	-17.58
15	-	-	-	172.0	3296.75	-17.70
16	-	-	-	190.0	3296.63	-17.82

8. Hanna SM. Magnetic Field Sensors Based on SAW Propagation in Magnetic Films, IEEE TRANSACTIONS ON ULTRASONICS, FERROELECTRICS, AND FREQUENCY CONTROL, VOL. UFFC-34, NO. 2, MARCH, 1987;PMID: 18290108. Available from: https://doi.org/10.1109/T-UFFC.1987.26931.
9. Wang JH, GUO R. Finite Element Simulation of Magnetostrictive and Piezoelectric Coupling in a Layered Structure, Taylor & Francis Group, 2007;Available from: https://doi.org/10.1109/ISAF.2008.4693786.
10. Chen L, Li P. The magnetostrictive material effects on magnetic field sensitivity for magnetoelectric sensor, Journal of Applied Physics, 2012;Available from: https://doi.org/10.1063/1.3670607.
11. Elhosni M, Elmazria O. FEM modeling of Multilayer Piezomagnetic Structure Based Surface Acoustic Wave Devices for Magnetic Sensor, ELSEVIER, EUROSENSOR 2014;Available from: https://doi.org/10.1016/j.proeng.2014.11.276.
12. Trang H, et al. Trade-Off between Issues in AlN/SiO2/Si Pressure Sensor, MEMSTECH'2007, May 23-26, 2007, Lviv-Polyana, UKRAINE;Available from: https://doi.org/10.1109/MEMSTECH.2007.4283449.
13. Morales AL, Nieto AJ. Simultaneous Measurement of Young's Modulus and Damping Dependence on Magnetic Fields by Laser Interferometry, In Proceedings of the International Conference on Thermal, Mechanical and Multi-Physics Simulation Experiments in Microelectronics and Micro-Systems, London, UK, 16-18 April 2007;Available from: https://doi.org/10.1109/ESIME.2007.360046.
14. Balymov KG, Kudyukov EV. Elastomagnetoresistive Properties of Films of 3d-Metalls Alloys, KnE Materials Science, ASRTU Conference Proceedings, 2016;Available from: https://doi.org/10.18502/kms.v1i1.555.
15. Ha TM, Hong HS. Modeling the selectivity of SAW filter with single phase unidirectional transducer based on FEM and equivalent circuit model, (MCA) Measurement, Control, and Automation, 2021;.
16. Hong HS, Mô phỏng bộ cộng hưởng sóng âm bề mặt có cấu trúc hai lớp sử dụng phuong pháp phần tử hữu hạn. Chuyên san Kỹ thuật Điều khiển và Tự động hóa, trang 31-36, 2015;.
17. Ha TM, Truyện NT, Phuong NH, Toán NV, Hồng HS. Nghiên cứu thiết kế bộ lọc và bộ cộng hưởng cao tần kiểu sóng âm bề mặt, Tạp chí Nghiên cứu KH&CN quân sự. 2017;52:89–96.
18. Auld BA. Acoustic Fields and Waves in Solids, John Wiley & Sons: New York, London, Toronto,Canada, Volume 1 and Volume 2, 1973;.
19. Massaro A, Cingolani R, Passases A. 3D FEM Modeling and Technology of Piezoelectric Ring Mems Antenna, Progress In Electromagnetics Research C, Vol. 23, 2011;Available from: https://doi.org/10.2528/PIERC11063003.
20. kumr Pati R, et al. SURFACE ACOUSTICS WAVE SENSOR BY USING PIEZOELECTRIC DEVICES, the Proceedings of the 2013 COMSOL Conference in Bangalore;.
21. Ya V. Shurural State university, russia, Lithium niobate and lithium tantalate-based piezoelectric materials, Woodhead Publishing Limited, 2010;Available from: https://doi.org/10.1533/9781845699758.1.204.
22. Andrushchak AS, Mytsyk BG. Complete sets of elastic constants and photoelastic coefficients of pure and MgO-doped lithium niobate crystals at room temperature, Citation: J. Appl. Phys. 2009;106:073510. Available from: https://doi.org/10.1063/1.3238507.
23. Morgan DP. Elastic Waves in Solid I, Free and Guided Propagation, Springer -Verlag Berlin Heidelberg 2000;.
24. Royer D, Dieulesaint E. Rayleigh velocity and displacement in orthorhombic, tetragonal, hexagonal, and cubic crystals, J.Acoust. Soc. Am. 76(5), November 1984;Available from:

https://doi.org/10.1121/1.391427.
25. Caliendo C, Verona E, Anisimkin VI. Surface acoustic wave humidity sensors: a comparison between different types of sensitive membrane, IOP science, 1997;Available from: https://doi.org/10.1088/0964-1726/6/6/007.

Tạp chí Phát triển Khoa học và Công nghệ – Engineering and Technology, 5(2):1426-1436

Open Access Full Text Article

Research article

Mô phỏng sự ảnh hưởng của đế áp điện đến đặc tính làm việc của cảm biến từ dạng SAW trên cơ sở vật liệu nhạy từ FeNi

Đỗ Duy Phú[1,2,*], Hoàng Sĩ Hồng[1,*], Lê Văn Vinh[3]

Use your smartphone to scan this QR code and download this article

TÓM TẮT

Bài báo mô phỏng sự ảnh hưởng của hai loại đế áp điện đến độ nhạy và khoảng làm việc của cảm biến từ giảo dạng SAW (SAW-MO: Surface Acoustic Wave - Magnetostriction) bằng phương pháp các phần tử hữu hạn (FEM: Finite Elements Method) trên cơ sở sử dụng lớp nhạy từ FeNi với đặc tính E-H (Module Young – Cường độ từ trường) đặc trưng. Cấu trúc cảm biến được lựa chọn để nghiên cứu là dạng delay-line: khoảng cách giữa hai bộ điện cực là 5mm, số cặp ngón tay của mỗi bộ điện cực là 25 và khoảng cách- độ rộng giữa các ngón tay đều nhau là 10mm, vật liệu làm điện cực là nhôm. Các đế áp điện được chọn để mô phỏng là $LiNbO_3$ và AlN. Trong đó đế áp điện $LiNBO_3$ là dạng khối với vận tốc sóng bề mặt là 3318.1m/s và AlN là dạng màng mỏng với vận tốc sóng bề mặt là 5598.9m/s. Do đó, tính tổng quát được bảo đảm khi đánh giá sự ảnh hưởng của chúng đến đáp ứng của cảm biến từ SAW-MO. Đối với vật liệu nhạy từ, nhóm lựa chọn FeNi với đặc tính E-H được xây dựng bằng thực nghiệm. Trong quá trình mô phỏng bằng phương pháp phần tử hữu hạn, cấu trúc cảm biến được thử nghiệm bằng nhiều bộ số liệu với tổng số phần tử được chia khác nhau. Tuy nhiên kết quả mô phỏng đã hội tụ với số phần tử được chia là 113556. Kết quả mô phỏng chỉ ra với cấu trúc cảm biến từ FeNi/IDT/AlN có độ nhạy cao hơn cấu trúc cảm biến từ FeNi/IDT/$LiNbO_3$ với độ nhạy tương ứng lần lượt là 8.698kHz/Oe và 2.345kHz/Oe. Kết quả mô phỏng còn cho thấy dải đáp ứng của cảm biến từ có cấu trúc FeNi/IDT/AlN là [0 ÷ 109]Oe nhỏ hơn so với cấu trúc FeNi/IDT/$LiNbO_3$ là [0 ÷ 190]Oe.

Từ khoá: SAW, FEM, Sóng âm bền mặt, Phường pháp các phần tử hữu hạn, Sóng âm bề mặt-từ giảo, Đặc tính cảm biến SAW-MO

[1]*Trường Điện - Điện tử, Trường Đại học Bách khoa Hà Nội, Hà Nội, Việt Nam*

[2]*Trường Đại học Công nghiệp Hà Nội, Hà Nội, Việt Nam*

[3]*Trường Đại học Phenikaa, Hà Nội, Việt Nam*

Liên hệ

Đỗ Duy Phú, Trường Điện - Điện tử, Trường Đại học Bách khoa Hà Nội, Hà Nội, Việt Nam

Trường Đại học Công nghiệp Hà Nội, Hà Nội, Việt Nam

Email: doduyphu@haui.edu.vn

Liên hệ

Hoàng Sĩ Hồng, Trường Điện - Điện tử, Trường Đại học Bách khoa Hà Nội, Hà Nội, Việt Nam

Email: hong.hoangsy@hust.edu.vn

Lịch sử

- Ngày nhận: 22-11-2021
- Ngày chấp nhận: 26-4-2022
- Ngày đăng: 30-6-2022

DOI : 10.32508/stdjet.v5i2.945

Check for updates

VNUHCM PRESS
25 years of scholarly publishing
1997-2022

Trích dẫn bài báo này: Phú D D, Hồng H S, Vinh L V. **Mô phỏng sự ảnh hưởng của đế áp điện đến đặc tính làm việc của cảm biến từ dạng SAW trên cơ sở vật liệu nhạy từ FeNi**. *Sci. Tech. Dev. J. - Eng. Tech.;* 5(2):1426-1436.